

Flood risk assessment of the naeseongcheon stream basin, Korea using the grid-based flood risk index

Won-joon Wang^a, Donghyun Kim^a, Gilho Kim^b, Kyung Tak Kim^b, Soojun Kim^a, Hung Soo Kim^{a,*}

^a Department of Civil Engineering, Inha University, Incheon, South Korea

^b Korea Institute of Civil Engineering and Building Technology, Ilsan, South Korea

ARTICLE INFO

Keywords:

Flood risk assessment
Grid data
Flood risk map
Indicator-based approach (IBA)
Flood damage rate

ABSTRACT

Study Region: Naeseongcheon Stream Basin, Korea

Study focus: We conducted a flood risk assessment using grid data for each indicator and a flood risk map. Using a grid-based flood risk map, grid data for the nine indicators included in the Hazard, Exposure, and Vulnerability items from 2016 to 2020 were selected and indexed by scoring each quantile interval. The entropy weight and Euclidean distance were then applied to calculate the grid-based item indices and flood risk index. Finally, the Expected Annual Damage (EAD) ranking calculated using the Korean flood risk assessment model was compared with the flood risk assessment ranking using grid data for 17 sub-basins in the Naeseongcheon Stream Basin for 2018.

New hydrological insights for the region: The analysis showed that the absolute error was improved by the application of the flood damage rate and selection of the grid cells including damage targets. When comparing the flood risk assessment ranking of each of the 17 sub-basins with the EAD ranking, the mean absolute error was 1.882, and the root mean square error was 3.009. This confirms that qualitative flood risk assessment using grid data and flood risk maps can provide as much basin-level risk analysis as quantitative flood risk assessment. Therefore, the method presented in this study can be utilized as a useful decision-support tool for the government's basin-level disaster prevention projects.

1. Introduction

In South Korea, large-scale flood damage caused by heavy rains and typhoons has been observed to occur every two years (2016, 2018, 2020, 2022). Local governments have thus established a River Improvement Master Plan (RIMP) as guidance for projects. To reduce the risk of flooding, river facilities, such as levees and drainage pumps, have been constructed. The government needs to efficiently use its limited disaster prevention budget and establish investment plans based on the results of economic analyses and qualitative flood risk assessments for each project area.

However, it is more difficult to obtain accurate results from flood risk assessments at the basin level than at the administrative level, such as in cities or counties. In practice, major statistical data such as the number of buildings, population, and farmland area are based on administrative boundaries such as city and county units; therefore, they cannot be applied to basins (Fekete, 2009; Fernandez et al.,

* Corresponding author.

E-mail address: sookim@inha.ac.kr (H.S. Kim).

2016; Bakkensen et al., 2017; Joo et al., 2019; Chen and Alexander, 2022; Kim et al., 2022). Even if applied, it is necessary to divide the number of buildings and population according to the area ratio of the administrative boundary overlapping with the basin, which makes it difficult to obtain accurate basin-level statistics.

Also, even if polygon-based spatial analysis data, such as land cover and soil maps, are used to extract the necessary data for each basin, the spatial analysis requires high work performance and considerable time. Recent basin-level flood risk assessments, such as grid-based rainfall data calculated using the kriging method, have introduced raster-based grid data with low workloads into flood risk assessments (Yu et al., 2018; Amadio et al., 2019; Park et al., 2019; Chen et al., 2021; Hwang et al., 2021). In general, the application of geostatistical methods, such as kriging, to the spatial distribution of rainfall grid units allows for unbiased predictions with minimal variance. It also has the advantage of considering the correlation between rainfall stations, thus enabling a gridded spatial distribution of rainfall (Biondi et al., 2021). However, when the number of rainfall stations included in the analysis increases, the time required for calculation increases compared with deterministic methods such as the Thiessen polygon method, and inverse distance weighting has the disadvantage that the analysis results may not be significantly improved over existing methods (Kurtzman et al., 2009; Ly et al., 2011; Yang et al., 2015; Chen et al., 2017). Typically, grid cell sizes such as 500 m × 500 m or 1 km × 1 km are mostly used for flood risk assessment, and statistical values such as rainfall, elevation, and the number of buildings are entered for each grid cell. Therefore, grid cells of the required area can be extracted and used for analysis without being restricted by administrative boundaries (European Forum for GeoStatistics, 2011; Steinnocher et al., 2011; Freire et al., 2016; Wang et al., 2020). By unifying the size and location of the grid cells for each indicator, the risk index can be easily calculated by combining the statistical values of the grid cells for each indicator located at the same coordinates.

Previous studies have combined grid data such as cumulative rainfall and elevation with regional statistics such as population density and GDP per capita to perform flood risk assessments (Lai et al., 2020; Zhang et al., 2020; Li et al., 2021). However, for grid-based risk analysis, all indicator-specific statistics must be reflected in the form of grid data. Gusyev et al. (2016) used administrative district-level statistics, such as population density, for grid data, where all grid cells in the region had the same population density. In addition, a flood risk assessment based on the inundation area and depth by basin was performed using grid-based flood risk maps created based on the flood peak discharge by frequency.

In flood risk assessments using grid data, an indicator-based approach (IBA) is commonly used to calculate flood risk indices (Benouar and Mimi, 2001; Han et al., 2015; NDMI, 2015; Lee et al., 2019). The IBA comprises four items (Hazard, Exposure, Vulnerability, and Capacity) and indicators that characterize each item. Previous studies on flood risk assessment sometimes included all four items, but sometimes only two or three items (Hazard, Exposure, and Vulnerability), depending on the scope of the target area and the availability of data for each indicator (Wannous and Velasquez, 2017). Once the indices of each indicator are calculated by indexing methods, such as min–max normalization, weights calculated by entropy weight and the analytic hierarchy process (AHP) are applied to calculate the itemized indices and flood risk index (Chuansheng et al., 2012; Kafle and Shakya, 2018; Lee et al., 2020; Aroca-Jiménez et al., 2022; Chen, 2022; Mousavi et al., 2022).

The aim of this study was to calculate a grid-level flood risk index using gridded flood risk maps of national and local rivers for 2016–2020 and grid data for each of the nine indicators included in the Hazard, Exposure, and Vulnerability items. First, the grid data for each indicator were selected using a flood risk map, and then the grid-level index for each indicator was calculated by scoring the sections using quantiles. Entropy weights were then applied to calculate each item index, and Euclidean distance was applied to calculate the grid-based flood risk index. In this study, only grid cells within the range of the flood risk map were selected and included in the analysis when reflecting the raw data of each grid cell using indicators such as maximum rainfall and number of buildings. The indicators included in the Exposure and Vulnerability items applied the flood damage rate to the grid cells overlaid with the flood risk map so that only objects that were actually exposed to flood risk could be reflected in the evaluation. Once the yearly grid-based flood risk index was calculated, it was screened again to exclude grid cells in which the number of buildings, population, and farmland areas were below the threshold. The calculated grid-based flood risk index was utilized not only as a statistical map but also for basin-level flood risk assessment. In this study, a flood risk assessment was conducted for 17 sub-basins of the Naeseongcheon Stream Basin in 2018 during the period to 2016–2020. The qualitative flood risk assessment ranking of each sub-basin derived from the analysis was compared with the quantitative flood risk assessment ranking to check for agreement based on absolute error. We aimed to develop a decision support tool that enables accurate and efficient qualitative flood risk assessment by extracting and aggregating only the target basin grid cells from the base-year flood risk index grid data.

2. Materials and methods

2.1. Procedure for assessing flood risk by basin using a grid-based flood risk index

The IBA method is commonly used to assess the qualitative risk for cities, counties, and countries using four items: Hazard, Exposure, Vulnerability, and Capacity, as well as the indicators associated with each item's characteristics (Park et al., 2005; Van Westen and Yifru, 2016; Wang et al., 2023). In flood risk assessment, the Hazard item consists of indicators that affect flood damage, such as rainfall and inundation areas. While the indicators in the Exposure item are composed of objects exposed to flood risk, the Vulnerability item consists of indicators that are more vulnerable to flood risk. Finally, Capacity comprises indicators that contribute to flood risk reduction.

In this study, national 500 m × 500 m grid data and grid-based national river and local river flood risk maps were used for each indicator of Hazard, Exposure, and Vulnerability to calculate the annual (2016–2020) grid-based flood risk index using IBA. The grid-based flood risk index consists of nine indicators: the Hazard item includes frequency-based rainfall (100-year frequency, duration

24 h, mm) and maximum rainfall (duration 24 h, mm); the Exposure item comprises the number of buildings (building), number of registered residents (people), official land value (1000 KW [Korean won]), and farmland area (m^2). Finally, the Vulnerability item consists of the number of old buildings (more than 20 years after construction; building), number of dependent people (population aged 7 and under, 65 and over; people), and field, greenhouse, and ginseng cultivation areas (m^2). The reason for using frequency-based rainfall and maximum rainfall as indicators for the Hazard item instead of flood discharge is that it is very difficult to construct grid-level flood discharge data for all the basins for each year. Therefore, we conducted a basin-level flood risk assessment using flood risk maps to compensate for the uncertainty in the assumption that grids with more rainfall will have more flood damage. In the case of Capacity, unlike the indicators of the other items, it is difficult to build the grid cells with individual attribute values. For example, when grid-based indicators are built from statistical data for each city and county, such as the density of disaster prevention facilities (pcs/km^2) and the ratio of the cumulative disaster prevention budget ($1000 KW/km^2$), all grid cells within a city have the same value. In this case, the flood risk index calculated by reflecting the Capacity item may have been overestimated or underestimated. Therefore, in this study, a basin-level flood risk assessment method that reflects only Hazard, Exposure, and Vulnerability items was developed.

The procedure for assessing the flood risk by basin using a grid-based flood risk index is summarized as follows:

1. The grid cells were selected by overlaying the indicator grid data for the Hazard, Exposure, and Vulnerability items on a flood risk map.
2. Indexing by indicators through scoring each quantile interval.
3. Apply entropy weighting to the indicator indices to calculate the item indices.
4. Apply min–max normalization to the item indices to unify the range between 0 and 1.
5. Apply Euclidean distance to calculate the grid-based flood risk index.
6. For each grid cell, exclude grid cells where the number of buildings, registered residents, and farmland areas were below the threshold.
7. Flood risk assessment by aggregating the grid-based flood risk indices by basin.

Fig. 1 shows the grid-based analysis procedure for the flood risk assessment.

2.2. Select grid data by indicator using grid-based flood risk maps

To calculate the national grid-based flood risk index, gridding was performed on the nine indicators of the three items. Frequency-based and maximum rainfall, which are indicators of the Hazard item, were gridded by applying kriging to point-by-point rainfall data from 69 automated synoptic observing system (ASOS) stations nationwide. For Exposure and Vulnerability items, the number of

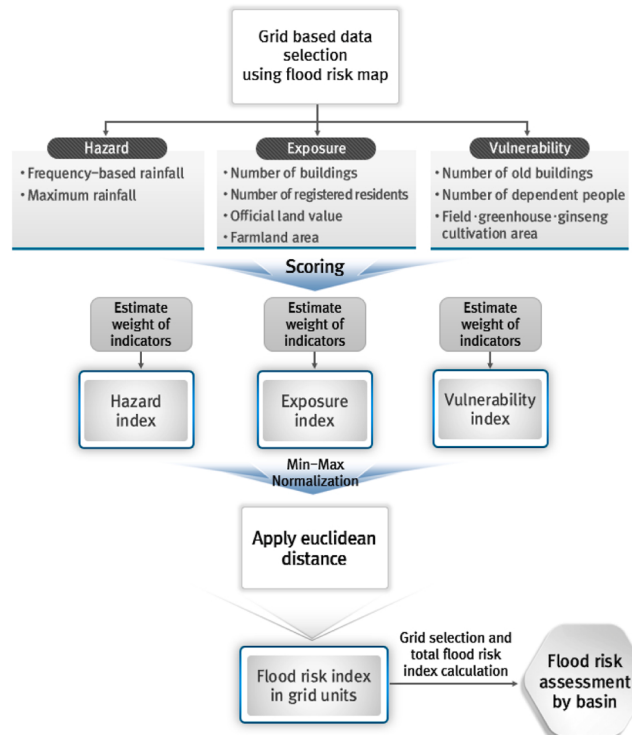


Fig. 1. Grid-based analysis procedure for flood risk assessment.

buildings, farmland areas, fields, greenhouses, and ginseng cultivation areas were gridded using high-resolution spatial analysis data, such as road name address electronic maps and smart farm maps. In addition, the number of registered residents, official land values, dependent people, and old buildings used grid data provided by the National Geographic Information Institute (NGII). The grid data for each indicator provided by the NGII are based on statistical and spatial analysis data collected and compiled by government departments. The grid data consisted of grid cells of various sizes, ranging from 100 m × 100 m to 100 km × 100 km, and grid-level statistics were updated monthly or quarterly to provide highly accurate grid data. Finally, nationwide grid data for Korea, consisting of 403,266 (500 m × 500 m) grid cells for each indicator, were created for each year, and the grid cells were selected by overlaying grid-based flood risk maps for national and local rivers. The flood risk map, which consists of 92,123 grid cells, uses the flood damage rate as an attribute value for each grid cell (Ministry of Construction and Transportation, 2004). For example, if a single 500 m × 500 m grid cell with an area of 250,000 m² has a flooded area of 200,000 m², the flood damage rate for the flood risk map grid cell would be 0.8. When extracting grid cells that overlapped with the grid-based flood risk map, the attribute values were modified by multiplying the attribute value of the grid cell by the flood damage rate of the flood risk map. If a particular grid cell with 10 buildings overlapped with a grid cell in the flood risk map with a flood damage rate of 0.6, the number of flooded buildings in the selected grid cell was six. Finally, the grid cells selected from the flood risk maps were modified by multiplying the flood damage rate with all indicator grid cells, except for frequency-based rainfall and maximum rainfall, which were unaffected by the flood damage rate. Figs. 2 and 3 show the national grid-level maximum rainfall and number of buildings as of 2020, as well as the grid data for the same indicators selected by the flood risk map. Fig. 4 shows an example of applying the flood damage rate when selecting the number of buildings (Grid) to be overlaid on the flood risk map.

2.3. Scoring each quantile interval

The nine indicators used to calculate the grid-based flood risk index were indexed after the selection was completed using a flood risk map. In general, qualitative risk assessments use methods such as min–max normalization and the t-score to perform indexing (Cai et al., 2016; Lyu et al., 2018; Jelinek et al., 2021). However, these methods skew the data distribution when there are very large maximum values, a small amount of data, or a very large number of specific values. If statistical values with such characteristics are used, the distribution of the index does not follow a normal distribution, and the final calculated flood risk index is distorted. To solve this problem, studies have attempted to reduce the deviation of statistical values by first applying a root transformation or log transformation to statistical values and then indexing. However, this approach has limitations. Fig. 5 shows the probability density function of the index calculated by applying simple min–max normalization and min–max normalization after root transformation of the number of grid-based buildings in the flood risk map. The number of grid cells of buildings by year selected by the flood risk map was 460,615 when all five years of grid cells were added together; however, there were 187,741 grid cells with fewer than one building, accounting for 40.758% of the total number. Therefore, it can be seen that the distribution of the data is skewed to the left even after applying the root transformation.

Indexing was performed by applying a grid-based scoring method using quantiles. The scoring method divides the statistics of each indicator into 10 intervals based on 10 quantiles and assigns a score to each interval in the range of 0.1. This method has the advantage of being able to index without skewing the distribution because scores are assigned to intervals of equal density. In this study, this method was applied to the Hazard, Exposure, and Vulnerability indicators to calculate the grid-level indices. However, in the case of the number of buildings indicator in the Exposure item, there were 187,741 (40.758%) grid cells with less than 1, which exceeded the fourth quantile; thus, the correct result could not be obtained if it was applied directly. Therefore, all grid cells with attribute values below the threshold in the Exposure and Vulnerability items were converted to 0.1 (number of buildings, number of people is less than 1, official land value is 0 [1000 KW], and farmland area is less than 2500 m² [1% of the single grid cell area]). Subsequently, the remaining grid cells for each indicator were divided into nine equal parts based on the nine quantiles, and scores were assigned at

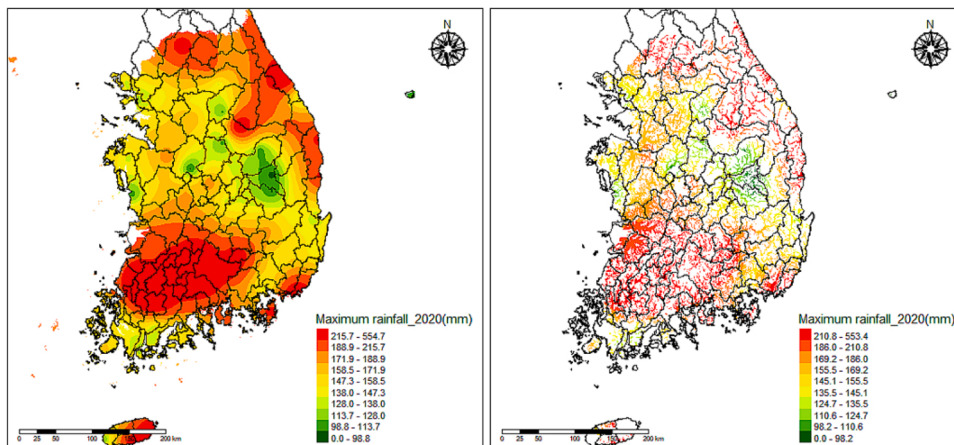


Fig. 2. National grid-based maximum rainfall for 2020 (left) and maximum rainfall within the flood risk map (right).

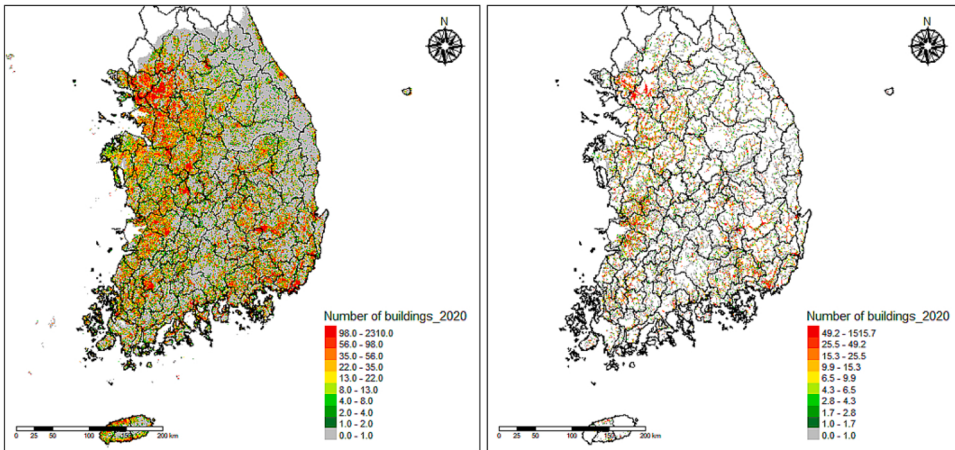


Fig. 3. The number of buildings on the national grid in 2020 (left) and the number of buildings within the flood risk map (right).

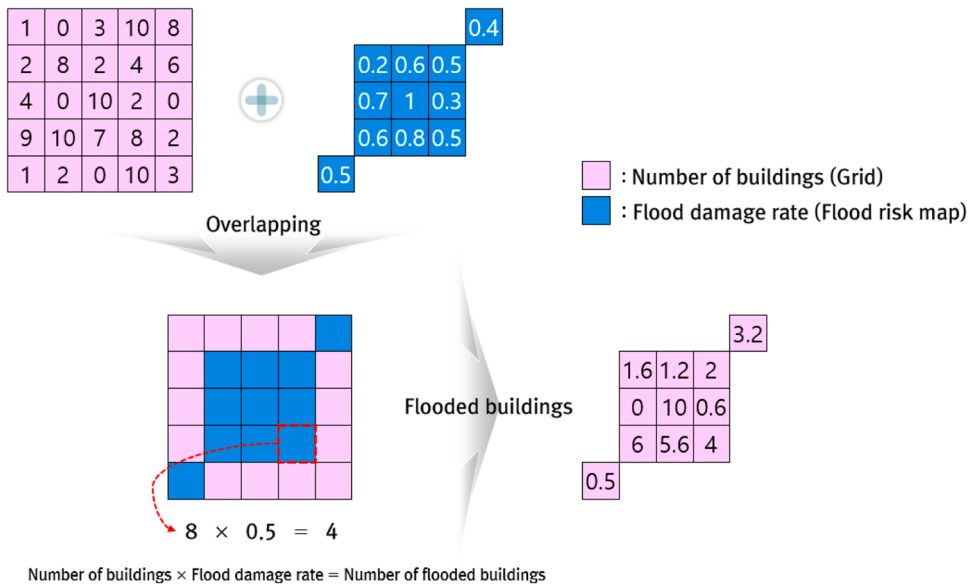


Fig. 4. Number of buildings (Grid), flood damage rate (Flood risk map), and number of flooded buildings.

intervals of 0.1, ranging from 0.2 to 1. Fig. 6 shows the grid-based number of buildings in the flood risk map scored on a scale of 0.2–1. It can be seen that all grid cells were scored at the same density except for those below the threshold, which is converted to 0.1.

2.4. Entropy weights and Euclidean distance

Once the indexing of the nine indicators was complete, entropic weights were applied to each indicator to calculate the item indices. The entropy weight was calculated using the quantitative characteristics of the statistical data. The weights calculated by the AHP or Delphi methods reflect the subjective opinions of experts participating in the survey. However, entropy weights have the advantage of obtaining objective results because they are calculated using statistical techniques (Al-Aomar, 2010; Lee et al., 2015; Seong and Byun, 2016). To calculate the entropy weight, Eqs. (1) and (2) index the raw data of each indicator using a matrix, whereas Eq. (3) calculates the entropy using the index of each indicator. Finally, Eqs. (4) and (5) were used to calculate the weight of each indicator using entropy.

$$D = \begin{bmatrix} x_{11} & \dots & x_{1n} \\ \vdots & \ddots & \vdots \\ x_{m1} & \dots & x_{mn} \end{bmatrix} \quad (1)$$

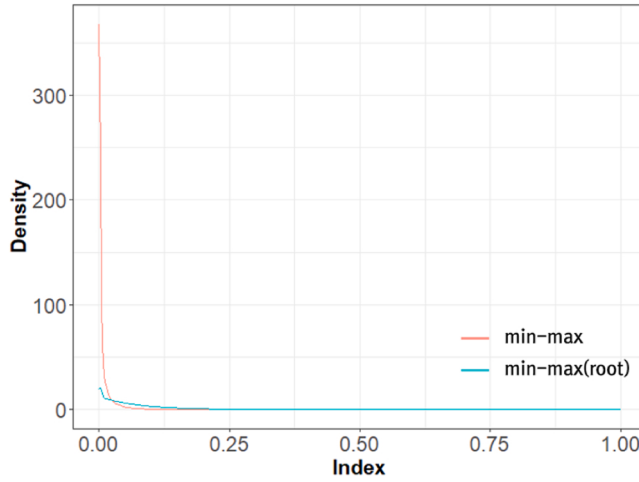


Fig. 5. Min–max normalized index of the number of grid-based buildings in the flood risk map.

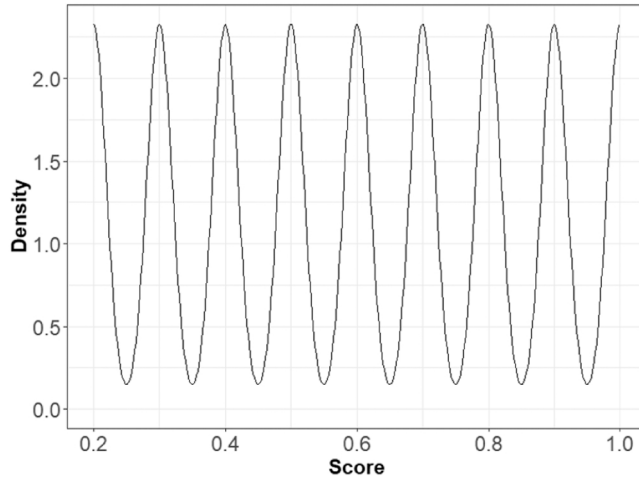


Fig. 6. Scoring each quantile interval of the number of grid-based buildings in the flood risk map.

$$p_{ij} = \frac{x_{ij}}{\sum_{i=1}^m x_{ij}} \quad (i = 1, 2, \dots, m; j = 1, 2, \dots, n) \quad (2)$$

$$E_j = -k \sum_{i=1}^m p_{ij} \log p_{ij} \quad (k = \frac{1}{\log m}; j = 1, 2, \dots, n) \quad (3)$$

$$d_j = 1 - E_j \quad (4)$$

$$w_j = \frac{d_j}{\sum_{j=1}^n d_j} \quad (j = 1, 2, \dots, n) \quad (5)$$

m: The number of grid cells

x_{ij}: Raw data by indicators

E_j: Entropy

w_j: Entropy weight

n: The number of indicators per item

p_{ij}: Normalized values

d_j: Attribute value diversity by indicators

Once the item indices were calculated by applying entropy weights to the indicator indices, min–max normalization was applied to the item indices to convert them into indices ranging from 0 to 1 before using the Euclidean distance. The Euclidean distance is a

method used to calculate the distance between two points and can be used not only for similarity analysis but also as an equal-weighting technique. In this study, Euclidean distance was applied to the Hazard, Exposure, and Vulnerability indices, as shown in Eq. (6), to calculate a grid-based flood risk index ranging from 0 to $\sqrt{3}$.

$$D = \sqrt{(Hazard)^2 + (Exposure)^2 + (Vulnerability)^2} \quad (6)$$

2.5. Assessment of flood risk in each basin

Once the grid-based flood risk indices within the flood risk map were calculated, the grid-based flood risk indices within the target basin boundaries were aggregated for basin-level flood risk assessment. The reason for aggregating rather than averaging grid-based flood risk indices within a basin is shown in Fig. 7. Basin A has two grid cells with a flood risk index of 1.7, and Basin B has 16 grid cells with a flood risk index of 1.4. Averaging the flood risk index for each grid cell in the two basins resulted in a greater flood risk in Basin A. However, logically, the risk in Basin B, which had a wider inundation area, was inevitably greater. Therefore, in this study, a basin-level flood risk assessment was performed by applying the sum, instead of the average, flood risk indices for each grid cell in the basin.

Before aggregating or taking the sum of the flood risk indices for each grid cell in the basin, it was necessary to select only the grid cells where flood-risk objects, such as buildings, population, and farmland, existed (see Fig. 8). This is because if all grid cells within the flood risk maps are included in the risk assessment, basins without flood risk objects may have an overestimated flood risk owing to their large inundation area. The criteria for determining which grid cells to exclude were as follows: (1) number of buildings, (2) population within the inundated grid cell less than 1, and (3) farmland area less than 2500 m². It should be noted that all three aforementioned conditions should be met in order for the grid cells to be excluded. By excluding all such grid cells in the basin and aggregating the flood risk indices of the remaining grid cells, the results required for the basin-level flood risk assessment can be obtained.

2.6. Korean flood risk assessment model

The Korean flood risk assessment model (K-FRM) is a loss assessment model for floods developed through research and development by the Ministry of the Interior and Safety (MOIS). This model is similar to the loss assessment models for natural disasters, such as Hazus-MH (Reese and Ramsay, 2010) and RiskScape (MOCT, 2004; Choi et al., 2006a; Choi et al., 2006b; Scawthorn et al., 2006; MOIS, 2020). The K-FRM uses high-resolution spatial analysis data on buildings, farmland, vehicles, and population, as well as flood risk maps, to calculate flood damage. In addition, the model builds a depth-damage function suitable for use in Korea through collaboration with insurance companies and expert consultation, enabling improved quantitative flood risk assessment compared with existing loss assessment models.

In this study, the results of the qualitative flood risk assessment calculated for the 17 sub-basins in the Naeseongcheon Stream Basin were compared with the expected annual damage (EAD) by sub-basin calculated using K-FRM. The EAD is the sum of the estimated damage that can occur in a flood event by frequency. A comparison with the EAD allowed us to check whether the qualitative flood risk ranking of each basin was consistent with the quantitative flood risk ranking. This comparison will also be the basis for analyzing the reasons for these differences. Fig. 9 shows the basic structure of the K-FRM.

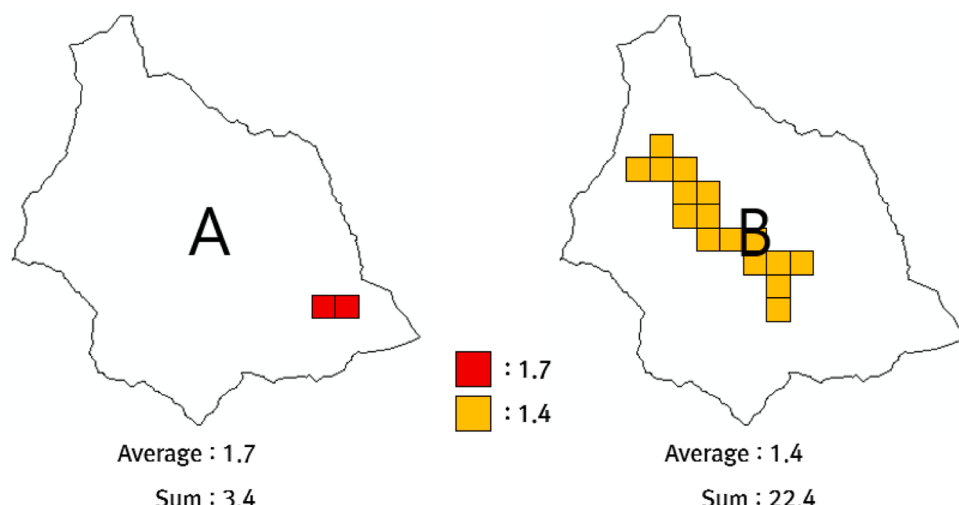


Fig. 7. Comparison of the average and the aggregated grid-based flood risk indices by basin.

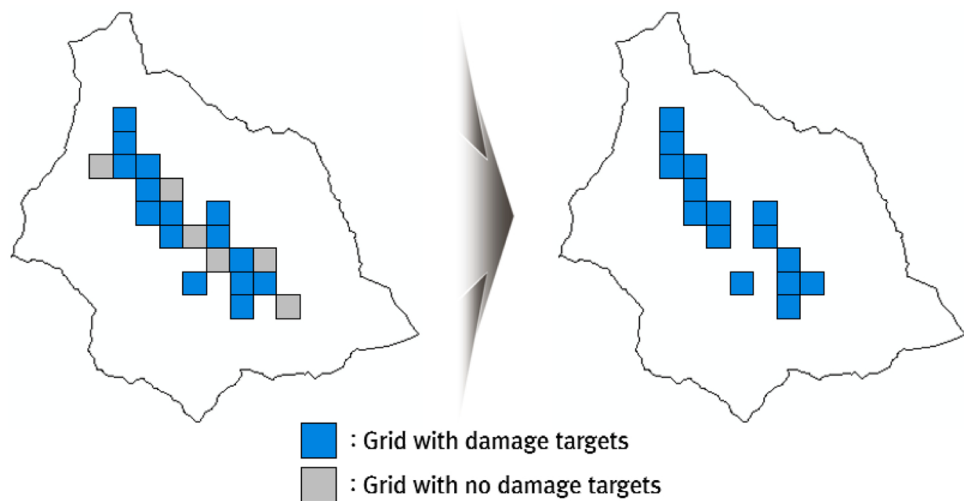


Fig. 8. Selection of flood risk index grid cells with flood risk objects.

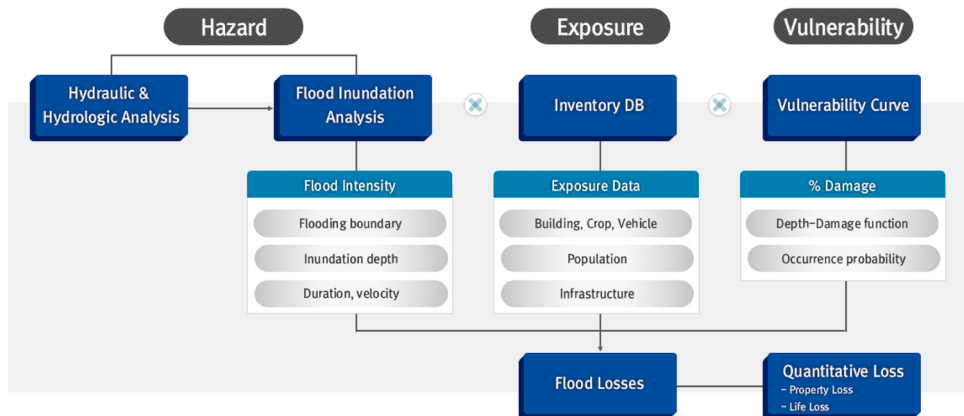


Fig. 9. K-FRM basic structure.

3. Application and results

3.1. Hydrometeorological characteristics of the study area

The Naeseongcheon Stream Basin is a mid-sized basin with 17 sub-basins located between $128^{\circ} 10'$ – $128^{\circ} 52'$ longitude and $36^{\circ} 32'$ – $37^{\circ} 03'$ latitude. The Naeseongcheon Stream, a tributary of one of the national Nakdong Rivers, is located within the basin area (Kim and Lee, 2014; Lee and Kim, 2017). The Naeseongcheon Stream Basin covers a total area of 1814.71 km^2 and has mountainous terrain, including the Sobaeck Mountains in the northern part. This stream basin has an average elevation of 318.2 m. Within the basin, the Naeseongcheon Stream flows in a northeastern to southwestern direction, and the average river width is widest downstream and narrowest midstream. Buildings and populations are concentrated in the downtown area, where the Yeongju City Hall and subway station are located, and streams such as the Seocheon Stream and Namwoncheon Stream flow across the city center. In terms of farmland, the upstream of the Naeseongcheon Stream includes fields of corn, potatoes, and highland vegetables, while rice fields are widely distributed downstream.

The Naeseongcheon Stream Basin experienced heavy rain and typhoon damage of more than 100 million KRW per year owing to heavy rains recorded in 2017 and specifically owing to Typhoon Kong-rey in 2018. The high risk of direct exposure to flood damage is attributed to the presence of urban centers and farmlands around rivers. Therefore, it is necessary to conduct accurate flood risk assessments at the basin level to support decision-making in disaster prevention projects. Fig. 10 shows the distribution of buildings, farmland, and hydrogeographic features in the Naeseongcheon Stream Basin.

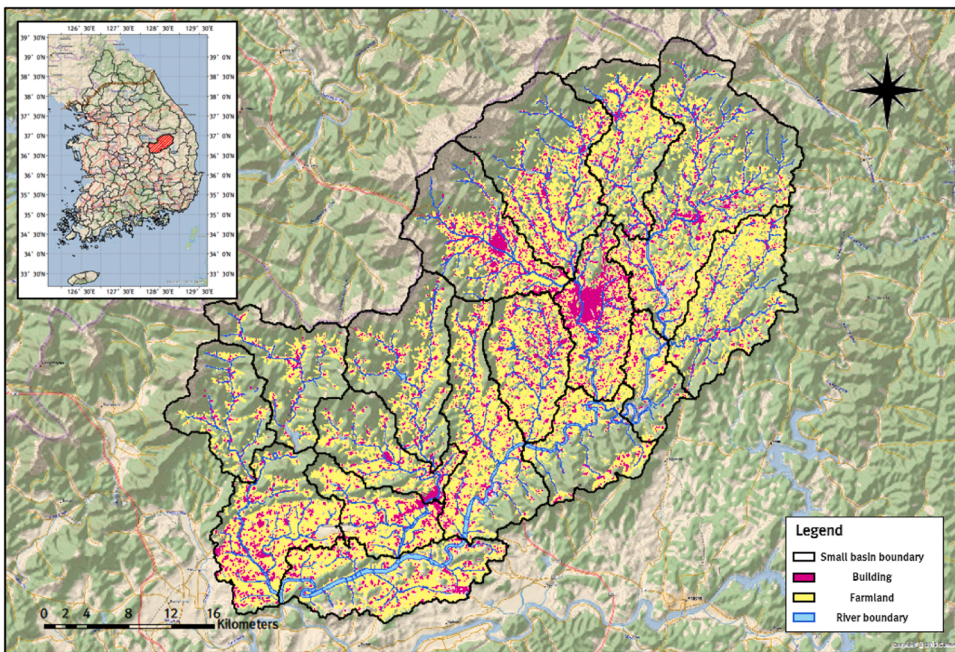


Fig. 10. Buildings, farmlands distribution, and hydrogeographic features of the Naeseongcheon Stream Basin.

3.2. Calculate a grid-based flood risk index

In this study, we calculated the flood risk index for each grid unit in the national flood risk map for 2016–2020 to evaluate the 2018 flood risk for each sub-basin in the Naeseongcheon Stream Basin. **Table 1** shows the entropy weight of each grid-level indicator used to calculate the item index. **Fig. 11** shows the grid-level items and flood risk indices by year in the national flood risk map.

In the case of the entropy weights for each indicator in **Table 1**, except for the indicators for the Hazard item, where the flood damage rate was not applied, there were differences in the weights calculated based on whether the flood damage rate was applied. When looking at the weight of each indicator in the three items, the maximum rainfall in the Hazard item, the number of registered residents and official land value in the Exposure item, and the number of old buildings and dependent people in the Vulnerability item had significantly high values.

Fig. 11 shows the changes in the grid-level item indices and the flood risk index by year. The change in the grid-level Hazard index by year was high because it was significantly affected by maximum rainfall. However, the changes in the indices of the Exposure and Vulnerability items were not high because the increases and decreases by year were low, given the characteristics of the indicators. The number of old buildings and dependent people, which are indicators of the Vulnerability item, are smaller than the indicators of the Exposure item; therefore, the Vulnerability index has a larger number of grid cells with a smaller index (dark green) than the Exposure index. Moreover, a grid cell with many registered residents and dependents indicated many residential buildings. Therefore, the Exposure and Vulnerability indices were calculated to be large for urban areas with dense buildings and populations. **Fig. 12** shows the item indices by grid unit calculated by applying the flood damage rate to the Naeseongcheon Stream Basin. In the figure, some grid cells in the sub-basins 200402 and 200407 have the Exposure and Vulnerability indices of more than 0.8, which means that buildings and population are concentrated.

Even in the Naeseongcheon Stream Basin, the number of grid cells with a Vulnerability index ranging from 0.0 to 0.1 was higher

Table 1
Calculation of entropy weights for each grid-level indicator.

Item	Indicator	Weight (No flood damage rate applied)	Weight (Flood damage rate applied)	Unit
Hazard	Frequency based rainfall	0.219	0.219	mm
	Maximum rainfall	0.781	0.781	mm
Exposure	Number of buildings	0.161	0.180	Building
	Number of registered residents	0.429	0.373	Person
	Official land price	0.348	0.329	1000 KW
Vulnerability	Area of farmland	0.062	0.118	m ²
	Number of old buildings	0.355	0.355	Building
	Number of dependent people	0.526	0.467	Person
	Field-greenhouse-ginseng cultivation area	0.109	0.178	m ²

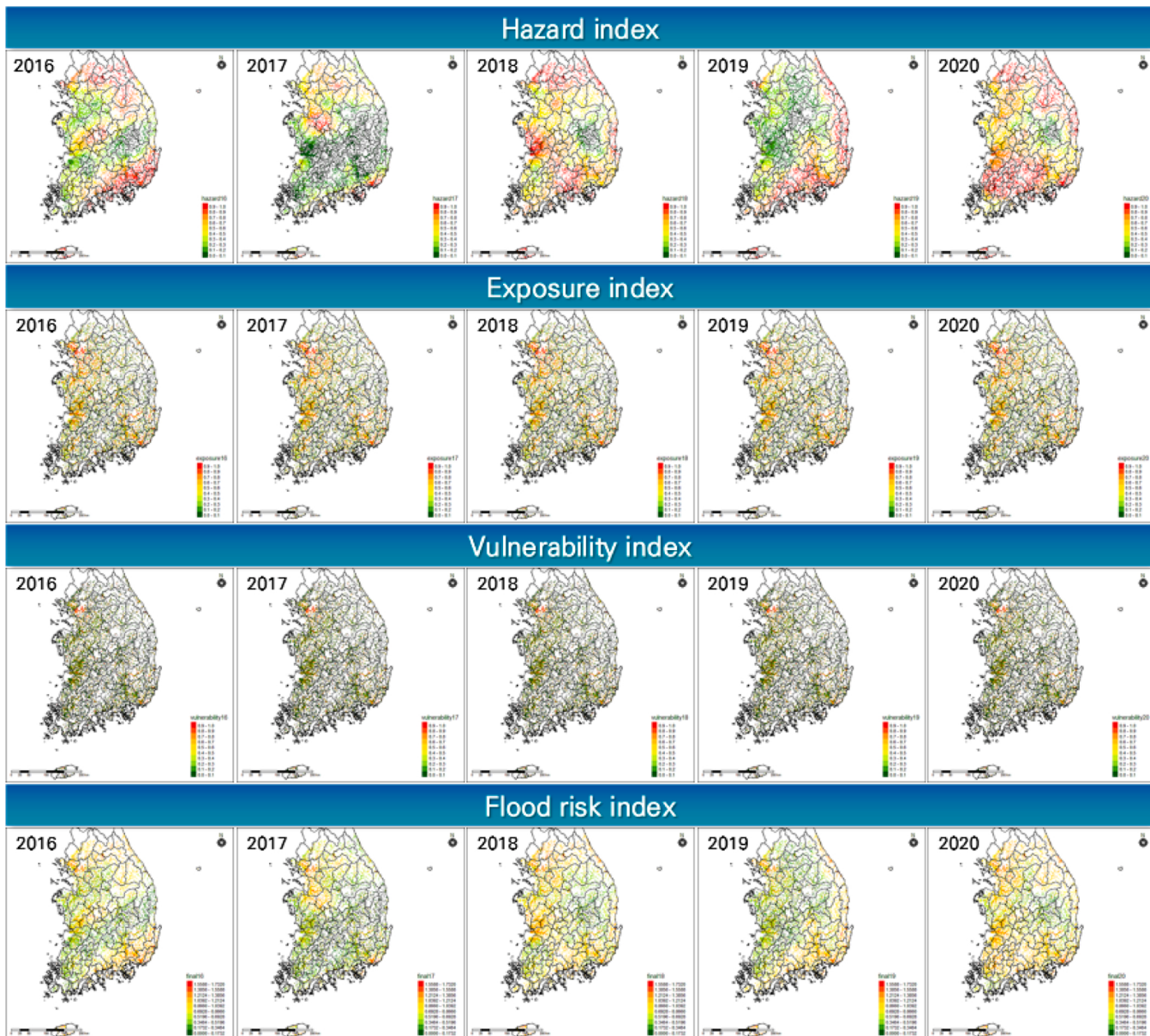


Fig. 11. Grid-based item indices and flood risk indices within the national flood risk map (2016–2020).

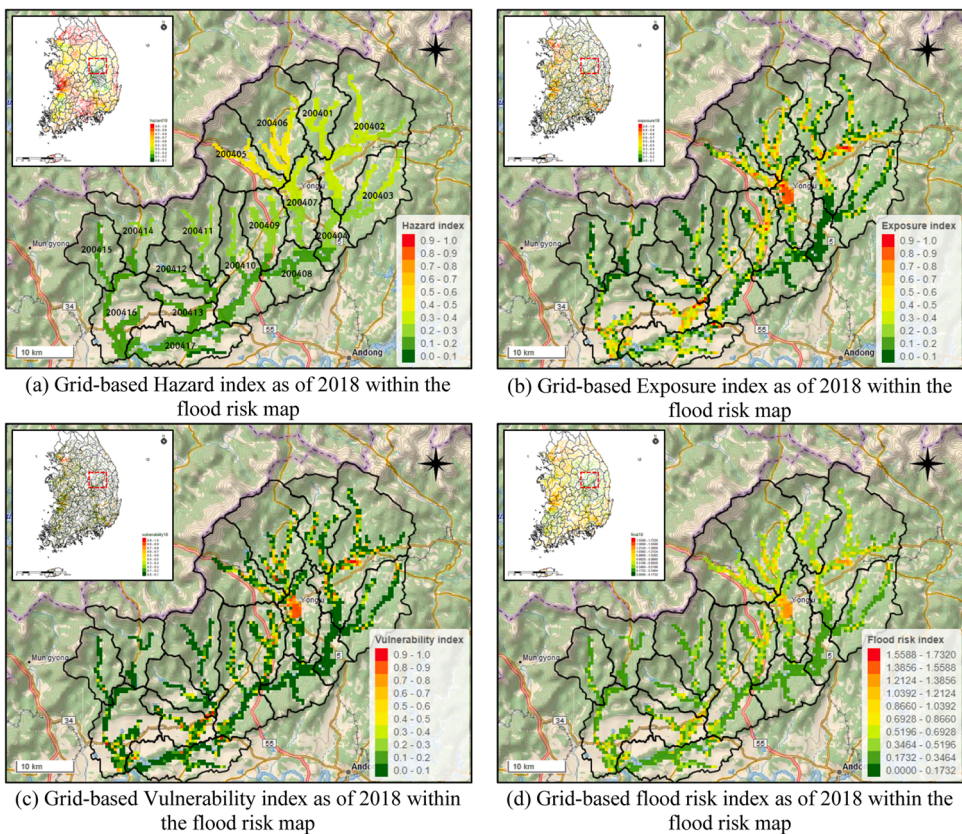


Fig. 12. Grid-based item indices and flood risk indices for 2018 within the Naeseongcheon Stream Basin.

than that with an Exposure index owing to the characteristics of the item. However, in the upstream areas of the Naeseongcheon Stream Basin, there were many grid cells with a large Vulnerability index. This was due to the growth of large areas of corn and highland vegetables. As for the Hazard index, as of 2018, the Naeseongcheon Stream Basin was less affected by extreme rainfall events than the other basins. However, the upper reaches of the Naeseongcheon Stream and the Sobaek Mountains experienced a certain level of rainfall owing to Typhoon Kong-rey. The grid-level flood risk index, which was calculated by applying the Euclidean distance to the item indices, was equally affected by each item index.

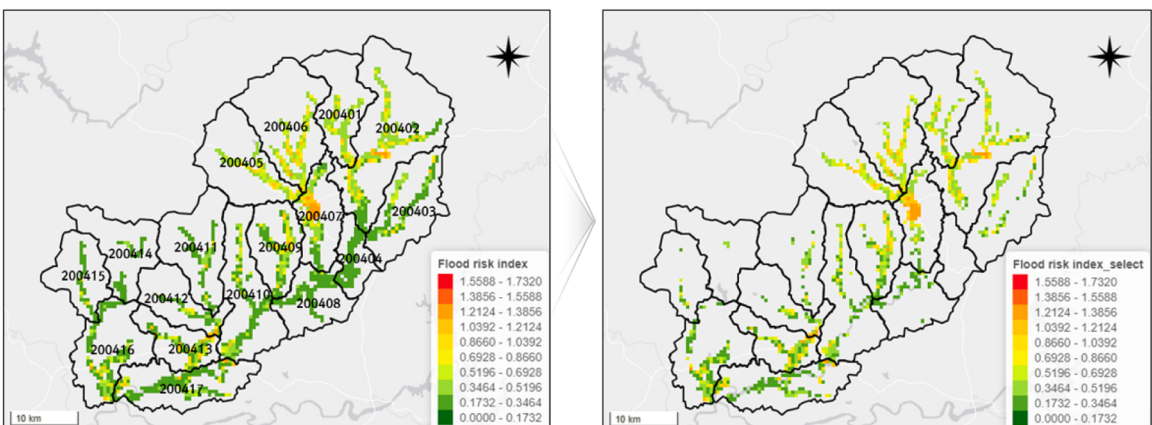


Fig. 13. Selected grid-based flood risk indices by sub-basins within the Naeseongcheon Stream Basin (2018).

3.3. Flood risk assessment results by sub-basins

For the 17 sub-basins included in the Naeseongcheon Stream Basin as of 2018, a basin-level flood risk assessment was performed using the grid-level flood risk index within the flood risk map. Before performing the basin-level flood risk assessment, grid cells with no buildings (fewer than one building), populations (fewer than one person), and farmland (less than 2500 m²) were removed by filtering. Fig. 13 shows the selected grid-level flood risk indices for the sub-basins in the 2018 Naeseongcheon Stream Basin.

The filtering process excluded a significant number of flood risk index grid cells from the Naeseongcheon Stream Basin. Most of the excluded grid cells had a flood risk index of less than 0.1732 (dark green). This means that they had no buildings, population, or farmland and, therefore, had a small flood risk index. For example, for sub-basin 200404, all existing grid cells in the sub-basin were excluded by filtering. The reason for this exclusion is that the watershed has a multipurpose dam, Yeongju Dam, which is built downstream. Residents who had lived along the river in the past in the sub-basin 200404 were relocated to other cities or higher ground within the basin and were not exposed to flood risks. Finally, the grid-based flood risk indices for each basin were aggregated to calculate the basin-level flood risk assessment results. In this study, the accuracy was evaluated based on the absolute error by comparing the basin-level flood risk assessment ranking with the quantitative flood risk assessment ranking calculated using K-FRM. For example, if the K-FRM ranking of a particular basin is 3 and the flood risk assessment ranking is 5, the deviation of the ranking is -2 and the absolute error is 2. Therefore, the smaller the absolute error per basin, the higher the agreement between the results of the K-FRM and the flood risk assessment. Table 2 compares the EAD ranking of each sub-basin calculated by applying the flood risk map by frequency (50, 80, 100, and 200 years) and K-FRM. The flood risk assessment ranking of each sub-basin was calculated by applying the flood damage rate and grid cells filtering. Fig. 14 shows the EAD and flood risk assessment rankings of the 17 sub-basins in the Naeseongcheon Stream Basin in 2018.

In the case of the EAD by sub-basin calculated using K-FRM, the flood damage amount was significant in sub-basins 200402, 200407, and 200412. In particular, in the case of 200407, where the EAD was calculated to be 6888.3 (1000 KW), a large urban center, including Yeongju City Hall, was exposed to flooding from the Seocheon Stream. In the assessment of flood risk by sub-basin, the absolute error between the EAD rankings was large, depending on the flood damage rate of the grid cell and the application of filtering for grid cell selection (Fig. 8). The analysis showed that the absolute error improved, especially when the flood damage rate was applied, compared with the application of grid cell filtering. It is also worth noting that the synergistic effect of applying both methods significantly reduced the absolute error of the basins. Compared with the EAD ranking, the sum of the absolute errors of the flood risk assessment ranking was calculated to be 32, the mean absolute error (MAE) was 1.882, and the root mean square error (RMSE) was 3.009. In particular, the flood risk assessment ranking showed a high consistency rate compared with the EAD ranking because the absolute error was 2 or less for all 17 sub-basins, except for sub-basins 200405, 200412, and 200417. This shows that, even in a qualitative flood risk assessment, it is possible to analyze basin-level risk as much as in a quantitative flood risk assessment by utilizing indicator grid data and flood risk maps.

Table 2
Comparison of EAD and flood risk assessment rankings by sub-basin.

Sub-basins	Flood damages (K-FRM)		No flood damage rate applied Selected grid cells			Flood damage rate applied Unselected grid cells			Flood damage rate applied Selected grid cells		
	EAD (1000 KW)	Rank	Sum of FRI	Rank	absolute error	Sum of FRI	Rank	absolute error	Sum of FRI	Rank	absolute error
200401	542.6	7	44.4	11	4	38.8	9	2	34.3	9	2
200402	2,699.5	2	118.0	1	1	98.5	1	1	78.9	1	1
200403	168	11	52.4	9	2	37.9	11	0	23.3	11	0
200404	0.3	17	13.8	16	1	16.0	15	2	0.0	17	0
200405	157.8	12	64.1	5	7	44.7	6	6	35.3	8	4
200406	650.1	4	79.4	2	2	66.2	2	2	57.9	2	2
200407	6,888.3	1	79.3	3	2	62.1	3	2	53.1	3	2
200408	20.8	15	27.1	14	1	17.7	13	2	8.9	14	1
200409	628.4	5	56.5	8	3	46.7	5	0	41.8	5	0
200410	250.5	9	58.8	7	2	40.5	8	1	33.8	10	1
200411	25.1	14	35.1	12	2	20.3	12	2	9.9	13	1
200412	675.4	3	29.2	13	10	17.3	14	11	13.6	12	9
200413	555	6	45.1	10	4	38.8	10	4	39.3	6	0
200414	1.1	16	13.1	17	1	8.8	17	1	1.0	16	0
200415	34.4	13	16.5	15	2	9.5	16	3	5.0	15	2
200416	424.3	8	66.5	4	4	42.7	7	1	39.0	7	1
200417	199.1	10	59.5	6	4	47.8	4	6	42.5	4	6
Sum of absolute error		52			46				32		
Mean absolute error (MAE)		3.058			2.705				1.882		
Root Mean Square Error (RMSE)		3.834			3.804				3.009		

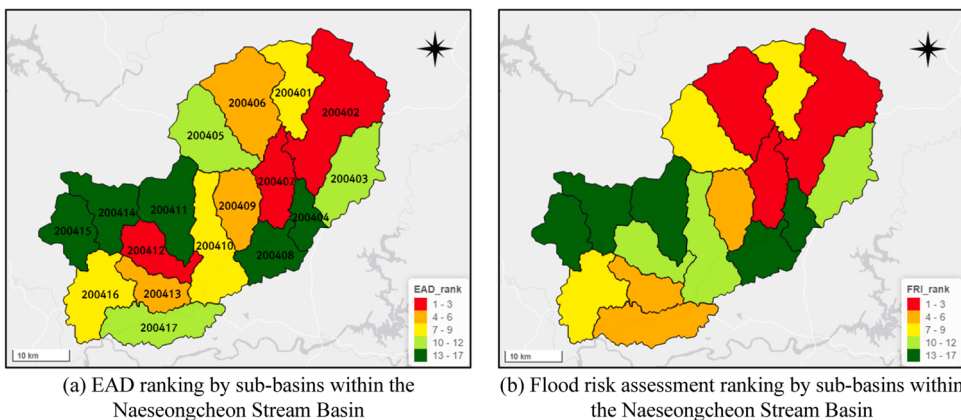


Fig. 14. Comparison of EAD and Flood Risk Assessment rankings by sub-basin in the Naeseongcheon Stream Basin in 2018.

4. Discussion

4.1. Comparison of results with and without the application of flood damage rate and grid cell filtering

Tables 3 and 4 show the sum of raw data by indicators in the Exposure and Vulnerability items and the number of grid cells selected according to whether the flood damage rate was applied by sub-basins in the Naeseongcheon Stream Basin.

These results can be used to understand the characteristics of each sub-basin. For example, in sub-basin 200402, the number of grid cells selected after applying the flood damage rate was 120, a reduction of 62 grid cells compared with 189 grid cells before selection. This suggests that, although the 200402 sub-basin had the largest inundated area among all the sub-basins, the flood damage rate and density of buildings, population, and farmland on the grid cells within the flood risk map were not high. In fact, when the flood damage rate was applied to the 200402 sub-basin, buildings were reduced by 75.5%, population by 68.9%, and farmland by 71.6% compared with the existing level. Therefore, when implementing disaster prevention projects in the 200402 sub-basin, it is necessary to establish a project execution plan for the area with the highest concentration of damaged targets within the scope of the inundation risk.

Although sub-basin 200407 was ranked at the top along with sub-basin 200402 in the flood risk assessment, the situation within the scope of the inundation risk was the opposite. For example, the number of grid cells selected without a flood damage rate was 97, which is the same as the number of grid cells before filtering. This means that none of the grid cells within the flood risk map were excluded because they had very high densities of buildings, population, and farmland. Therefore, it can be assumed that the number of selected grid cells decreased by 28 after applying the flood damage rate because approximately 28.8% of the flood risk map grid cells had a very small flood damage rate. In fact, Fig. 15 shows the distribution of buildings, farmland, and grid-level flood risk maps in the 200407 sub-basin; there are many flood risk map grid cells with very low flood damage rates both upstream and downstream of the river. Nevertheless, the 200407 sub-basin had a very high density of buildings and population, and in urban areas, the grid-level flood damage rate was very high, reaching approximately 0.901. Among the 17 sub-basins, the 200407 sub-basin ranked third in the EAD and first in the flood risk index. Therefore, when carrying out disaster prevention projects in the 200402 sub-basin, it is necessary to closely examine all areas within the flood risk maps and construct disaster prevention facilities with a high design frequency.

As mentioned earlier, the 200404 sub-basin, which ranks last in the flood risk assessment, has a multipurpose dam called the Yeongju Dam. This area had the smallest total number of buildings, population, and farmland area among the 17 sub-basins, and even without applying the flood damage rate, approximately 37.8% of the grid cells were already excluded. If the flood damage rate was applied, then the number of selected grid cells was zero. This is because people living in the sub-basin moved to higher ground or areas farther away from the river to avoid the risk of inundation caused by the dam. The distribution of buildings and farmland in Fig. 16 shows that they are located on higher ground or in areas farther from the river. Because the terrain around the river is steep, the attribute value of the grid cell with the largest flood damage rate within the flood risk map of the 200404 sub-basin was approximately 0.036. Therefore, grid cells with buildings, populations, and farmland within the flood risk map were excluded from the selection criteria when the flood damage rate was applied, and the final number of selected grid cells was zero.

4.2. Assessment of the causes for sub-basins with large absolute errors

In Table 2, comparing the EAD ranking and flood risk assessment ranking of each sub-basin, the absolute error of 14 of the 17 sub-basins is less than or equal to 2. However, the absolute errors of the remaining three sub-basins (200405, 200412, and 200417) were high.

The 200405 sub-basin is located at the beginning of the Sobaek Mountains and is similar to the 200404 sub-basin, which has a steep slope and narrow river. However, unlike the 200404 sub-basin, this sub-basin does not have a dam, which means that there is a large area of buildings and farmland along the river. In the event of a flood in the 200404 sub-basin, a long, thin strip of the flood risk map was drawn along the stream. The flood damage rates within the grid-based flood risk maps were higher around the farmland than in the

Table 3

Sum of grid-based raw data within flood risk maps by sub-basins (no flood damage rate was applied).

Sub-basins	Number of grid cells		Exposure				Vulnerability		
	Before selection	After selection	Number of buildings	Number of registered residents	Official land price (1000 KW)	Area of farmland	Number of old buildings	Number of dependent people	Field-greenhouse-ginseng cultivation area
200401	72	72	1,815	1,116	124,294,947	5,921,935	558	503	2,333,307
200402	189	182	5,733	10,085	571,009,750	13,001,639	2,424	3,163	4,973,576
200403	99	99	2,345	1,798	88,851,132	5,409,706	866	815	3,163,427
200404	66	41	184	301	71,783,450	691,930	9	99	557,857
200405	73	72	4,244	7,409	601,254,232	8,790,272	1,355	2,335	2,774,126
200406	105	105	3,993	2,776	284,775,855	11,581,376	1,278	1,158	3,920,480
200407	97	97	12,622	42,944	2,310,183,312	3,902,568	7,802	12,785	2,481,774
200408	84	83	1,253	543	74,041,687	3,250,558	293	245	1,927,626
200409	102	102	2,945	1,537	253,611,680	8,858,235	723	627	3,609,805
200410	117	117	3,151	1,814	295,751,582	9,426,659	827	879	3,342,842
200411	63	59	2,045	1,301	109,991,360	4,530,947	565	541	1,490,793
200412	43	43	4,268	7,122	493,789,905	3,188,882	1,746	2,377	1,094,734
200413	76	76	3,411	3,249	392,473,525	9,096,278	1,055	1,205	1,948,639
200414	37	29	765	441	51,509,657	1,444,063	235	172	1,128,923
200415	38	37	1,030	530	51,831,327	2,444,867	263	255	667,131
200416	121	119	4,929	2,940	370,729,877	13,764,021	1,578	1,340	2,767,194
200417	140	133	2,926	3,266	979,001,432	10,974,689	692	1,076	3,177,269

Table 4

Sum of grid-based raw data within flood risk maps by sub-basins (flood damage rate was applied).

Sub-basins	Number of grid cells		Exposure				Vulnerability		
	Before selection	After selection	Number of buildings	Number of registered residents	Official land price (1000 KW)	Area of farmland	Number of old buildings	Number of dependent people	Field-greenhouse-ginseng cultivation area
200401	72	55	448	284	38,972,340	1,767,012	147	120	571,717
200402	189	120	1,398	3,135	202,892,090	3,688,787	618	951	1,034,179
200403	99	48	256	196	9,285,533	576,696	91	88	296,472
200404	66	0	0	0	365,994	4,334	0	0	3,586
200405	73	53	337	458	61,821,134	1,488,853	103	144	349,870
200406	105	83	775	561	71,531,855	3,024,407	251	236	899,256
200407	97	69	5,796	18,862	1,089,345,462	795,668	4,273	5,870	362,921
200408	84	32	70	29	4,889,858	213,237	17	15	116,765
200409	102	77	668	365	68,040,715	2,511,220	172	142	703,750
200410	117	75	394	223	52,407,238	2,252,137	100	105	728,415
200411	63	23	114	90	7,993,995	353,935	33	38	103,383
200412	43	26	578	1,183	77,992,902	309,144	282	385	81,394
200413	76	67	824	767	138,151,959	3,804,912	228	284	498,035
200414	37	3	10	6	802,348	27,498	3	2	20,886
200415	38	12	91	43	4,352,715	201,932	23	23	54,193
200416	121	92	651	379	87,565,024	3,614,043	200	163	641,594
200417	140	97	615	344	107,959,078	3,215,211	150	148	974,188

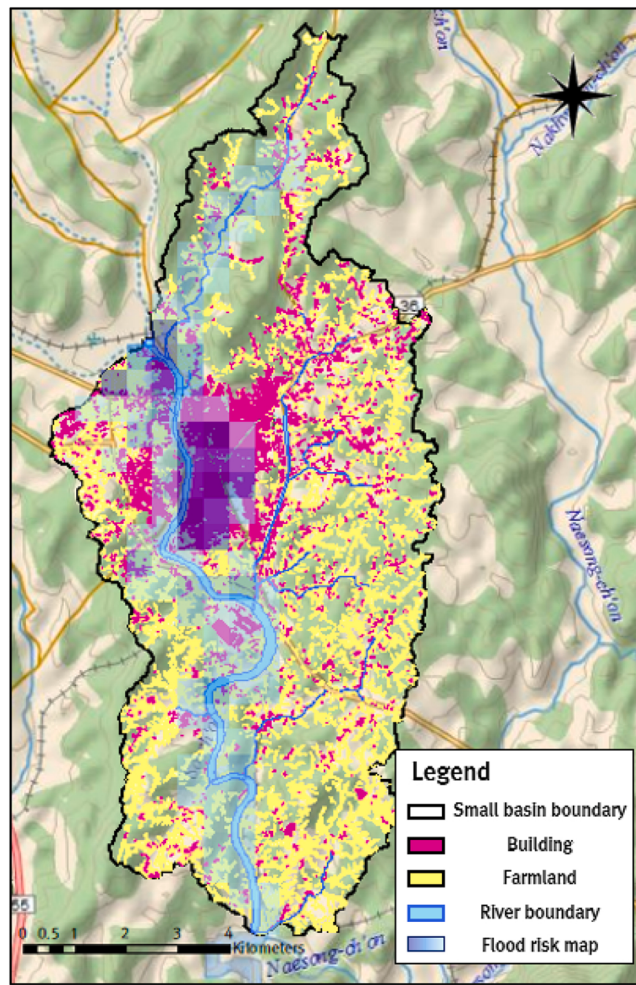


Fig. 15. Distribution of buildings, farmland, and grid-based flood risk maps in the 200407 sub-basin.

city center, where buildings were denser. Therefore, the EAD calculated for the 200405 sub-basin was 157.8 (1000 KW), which was smaller than the other sub-basins. This is because flooding occurs mainly on farmland, which has a smaller unit cost than buildings. However, in the flood risk assessment, many grid cells were not excluded because of the large areas of flooded farmland. Therefore, the flood risk assessment ranking was high compared with the EAD ranking, resulting in a large absolute error.

The characteristics observed in the 200405 sub-basin were the same as in the 200417 sub-basin. In Fig. 17, the distribution of buildings, farmland, and flood risk maps in the 200417 sub-basin shows that farmland is more widely distributed than buildings because of the development of plains around the main river and local tributaries. Therefore, in the event of a flood, farmlands located near rivers are primarily affected. Finally, the EAD of the 200417 sub-basin was 199.1 (1000 KW), which was ranked 10th. However, most grid cells were not excluded from the grid cell selection process, resulting in a flood risk index of 42.5, which was ranked 4th.

However, the 200412 sub-basin exhibited characteristics different from those of sub-basins 200405 and 200407. As shown in Fig. 18, the 200412 sub-basin, similar to the 200405 sub-basin, has a narrow river width. This is due to the mountainous nature of the sub-basin. The plain area is also small, except for a few midstream and downstream areas. This causes this sub-basin to have a smaller flood risk area and a higher building density around the river than the other sub-basins. However, most buildings are clustered midstream and downstream, and in the event of a flood, the flood damage rate is calculated to be higher in downstream urban centers than in farmlands. Thus, the EAD of the 200412 sub-basin was calculated to be 675.4 (1000 KW) or rank 3rd. However, the sum of the flood risk indices was calculated to be 13.6 (12th) because 17 of the 43 grid cells (approximately 39.5%) were excluded from the selection. Finally, the high concentration of high-value buildings downstream of the flooded areas and the small area of the flood risk map in the basin, which did not have sufficient grid cells to reflect the flood risk assessment, contributed to the large absolute error. In addition, in a quantitative flood risk assessment, the range of damage that can occur in individual grid cells is wide. However, the grid-level flood risk index is $0-\sqrt{3}$. Therefore, if the number of grid cells reflected in the flood risk assessment is low, the sum of the basin flood risk indices cannot increase.

This study utilized the results of a national grid-based flood risk index calculation to conduct a flood risk assessment for 17 sub-

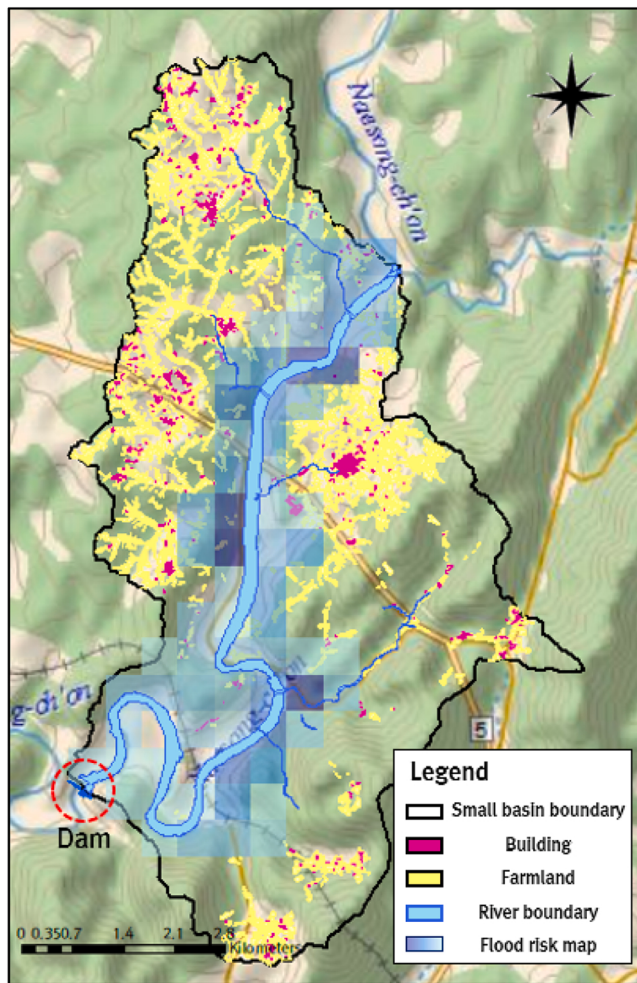


Fig. 16. Distribution of buildings, farmland, and grid-based flood risk maps in the 200404 sub-basin.

basins in the Naeseongcheon Stream Basin. In previous studies, statistical data aggregated by local governments and polygon-based spatial data analysis were used to conduct basin-level flood risk assessments, making it difficult to conduct accurate flood risk assessments by basin. However, when performing flood risk assessment for each of the 17 sub-basins of the Naeseongcheon Stream Basin using the method presented in this study, the sum of the absolute error was 32, MAE was 1.882, and RMSE was 3.009, which is very similar to the EAD ranking. In some basins, such as 200405, 200412, and 200417, the absolute error between the EADs was very high, confirming the limitations of the methodological approach. Nevertheless, because we were able to determine the cause of the problem by basin through the analysis, we could try to improve it by reestablishing the selection criteria of the grid data and modifying the weight of each indicator.

5. Conclusions

In this study, the grid-based flood risk index was calculated using the national grid-based spatial analysis data and flood risk maps for 2016–2020, and the grid-based flood risk index was used to evaluate the flood risk of each of the 17 sub-basins of the Naeseongcheon Stream Basin. The following implications can be derived from the analytical results of this study.

The first is the usefulness of the basin-level flood risk assessment using a grid-based flood risk index. In the existing qualitative flood risk assessment, it is difficult to accurately analyze basin-level flood risk because the assessment is conducted using administrative district-level statistics and surveys. In addition, quantitative risk assessment requires spatial analysis of each type of asset exposed to flood risk to calculate the amount of damage; therefore, the time and difficulty required for analysis are very high. However, the national grid-based flood risk index calculated in this study has no spatial constraints, and it is easy to perform a flood risk assessment because only the grid cell for the base year required for the analysis must be extracted and aggregated. Moreover, in the grid-based statistical map, the grid cells are displayed in different colors depending on the rainfall intensity, number of buildings, and farmland area, making it easier for decision-makers in disaster prevention projects to identify the risk situation by basin.

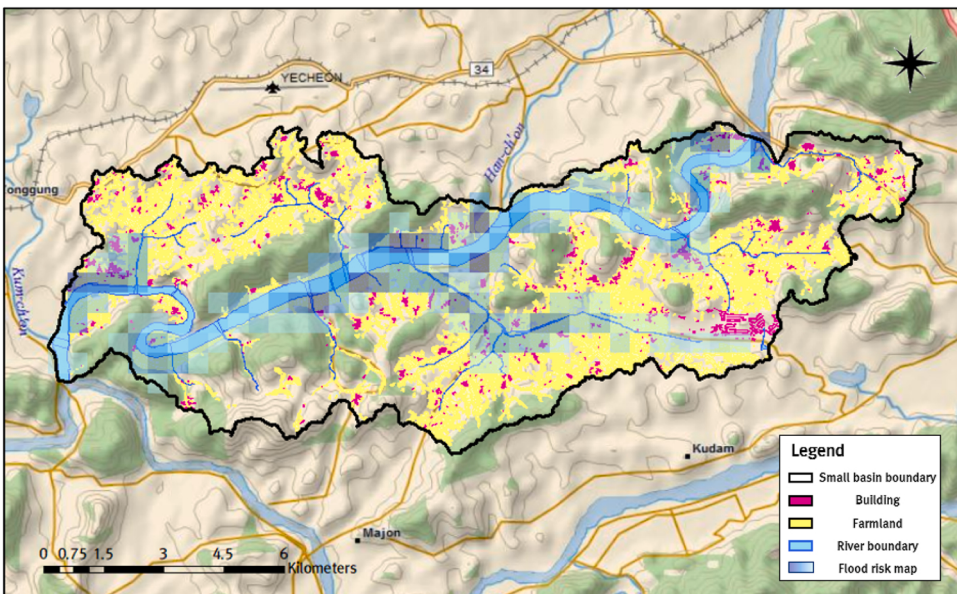


Fig. 17. Distribution of buildings, farmland, and grid-based flood risk maps in the 200417 sub-basin.

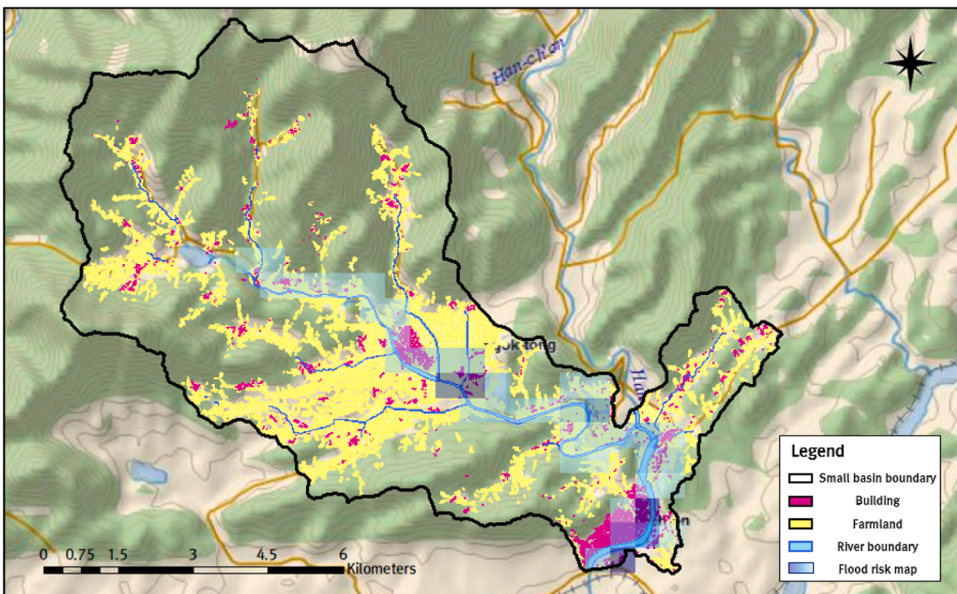


Fig. 18. Distribution of buildings, farmland, and grid-based flood risk maps in the 200412 sub-basin.

The second is the accuracy of the flood risk assessment, which has been improved by applying the flood damage rate and grid cell selection when performing the basin-level flood risk assessment using grid data. When conducting a qualitative flood risk assessment by basin, if all grid cells within the flood risk map are included in the assessment, the flood risk of a basin with a large inundated area would inevitably be large. Therefore, the flood damage rate was applied to modify the statistical value of each grid cell exposed to flood risk, and only the grid cells with damaged objects (buildings, population, and farmland) within the flood risk map were selected based on the selection criteria. As a result, the smallest absolute error was calculated compared with the EAD calculated using the K-FRM for the 17 sub-basins in the Naeseongcheon Stream Basin.

Third, basins with large absolute errors compared with the EAD revealed the limitations of qualitative flood risk assessment using the grid-based flood risk index. The flood risk indices that can be calculated for individual grid cells range from 0 to $\sqrt{3}$, which is much smaller than the variation in the grid-based damage calculated for each asset type in a quantitative flood risk assessment. Therefore, basins with a large farmland area within the flood risk map and many selected grid cells or basins with a small inundation area but a

high density of buildings within the flood risk map had large absolute errors in the EAD. This problem can be solved by reestablishing the selection criteria for grid cells within the flood risk map and adjusting the weight of each indicator.

The basin-level flood risk assessment method proposed in this study overcomes the limitations of existing studies by improving the accuracy and convenience of risk assessment. This method is expected to contribute to decision support for flood damage reduction, along with quantitative evaluations such as economic analysis of disaster prevention projects.

CRediT authorship contribution statement

Kim Kyung Tak: Software, Funding acquisition, Conceptualization. **Kim Gilho:** Resources, Formal analysis. **Kim Donghyun:** Visualization, Resources. **Wang Won-joon:** Writing – original draft, Visualization, Software, Methodology. **Kim Hung Soo:** Writing – review & editing, Project administration. **Kim Soojun:** Resources, Project administration.

Declaration of Competing Interest

The authors declare the following financial interests/personal relationships which may be considered as potential competing interests: Hung Soo Kim reports financial support was provided by Korea Environment Industry & Technology Institute.

Data Availability

Data will be made available on request.

Acknowledgements

This work was supported by Korea Environmental Industry&Technology Institute(KEITI) through R&D Program for Innovative Flood Protection Technologies against Climate Crisis Project, funded by Korea Ministry of Environment(MOE)(2022003460002). This research was supported by the KICT Research Program (Project No. 20230263–001).

References

- Al-Aomar, R., 2010. A combined ahp-entropy method for deriving subjective and objective criteria weights. *Int. J. Ind. Eng. Theory Appl.* Pr. 17, 12–24.
- Amadio, M., Mysiak, J., Marzi, S., 2019. Mapping socioeconomic exposure for flood risk assessment in Italy. *RISK ANAL* 39 (4), 829–845.
- Aroca-Jiménez, E., Bodoque, J.M., García, J.A., Figueira-García, J.E., 2022. Holistic characterization of flash flood Vulnerability: construction and validation of an integrated multidimensional Vulnerability index. *J. Hydrol.* 612, 128083.
- Bakkensen, L.A., Fox-Lent, C., Read, L.K., Linkov, I., 2017. Validating resilience and vulnerability indices in the context of natural disasters. *RISK ANAL* 37 (5), 982–1004.
- Benouar, D., & Mimi, A. (2001, August). Improving emergency management in Algeria. In Global alliance international workshop on disaster reduction, Reston, VA.
- Biondi, D., Greco, A., De Luca, D.L., 2021. Fixed-area vs storm-centered areal reduction factors: a Mediterranean case study. *J. Hydrol.* 595, 125654.
- Cai, H., Lam, N.S.N., Zou, L., Qiang, Y., Li, K., 2016. Assessing community resilience to coastal Hazards in the Lower Mississippi River Basin. *WATER-SUI* 8 (2), 46.
- Chen, J., Chen, W., Huang, G., 2021. Assessing urban pluvial flood resilience based on a novel grid-based quantification method that considers human risk perceptions. *J. Hydrol.* 601, 126601.
- Chen, T., Ren, L., Yuan, F., Yang, X., Jiang, S., Tang, T., Zhang, L., 2017. Comparison of spatial interpolation schemes for rainfall data and application in hydrological modeling. *Water* 9 (5), 342.
- Chen, Y., 2022. Flood Hazard zone mapping incorporating geographic information system (GIS) and multi-criteria analysis (MCA) techniques. *J. Hydrol.* 612, 128268.
- Chen, Y., Alexander, D., 2022. Integrated flood risk assessment of river basins: application in the dadu river basin, China. *J. Hydrol.* 613, 128456.
- Choi, S.A., Yi, C.S., Shim, M.P., Kim, H.S., 2006a. Multi-dimensional flood damage analysis (i): principle and procedure. *J. Korean Water Resour. Assoc.* 39 (1), 1–9.
- Choi, S.A., Yi, C.S., Shim, M.P., Kim, H.S., 2006b. Multi-dimensional flood damage analysis (ii): application. *J. Korea Water Resour. Assoc.* 39 (1), 11–22.
- Chuansheng, X., Dapeng, D., Shengping, H., Xin, X., Yingjie, C., 2012. Safety evaluation of smart grid based on AHP-entropy method. *Syst. Eng. Proc.* 4, 203–209.
- European Forum for GeoStatistics, 2011. Testing and quality assessment of pan-European population grid. Author, Stockholm, Sweden.
- Fekete, A., 2009. Validation of a social Vulnerability index in context to river-floods in Germany. *Nat. Hazard. Earth Syst.* 9 (2), 393–403.
- Fernandez, P., Mourato, S., Moreira, M., 2016. Social Vulnerability assessment of flood risk using GIS-based multicriteria decision analysis. A case study of Vila Nova de Gaia (Portugal). *Geomat. Nat. Haz. Risk* 7 (4), 1367–1389.
- Freire, S., MacManus, K., Pesaresi, M., Doxsey-Whitfield, E., Mills, J., 2016. Development of new open and free multi-temporal global population grids at 250 m resolution. *Population* 250.
- Gusyev, M., Gädeke, A., Cullmann, J., Magome, J., Sugiura, A., Sawano, H., Takeuchi, K., 2016. Connecting global-and local-scale flood risk assessment: a case study of the Rhine River basin flood Hazard. *J. Flood Risk Manag.* 9 (4), 343–354.
- Han, S.R., Kang, N.R., Lee, C.S., 2015. Disaster risk evaluation for urban areas under composite Hazard factors. *Kosham* 15 (3), 33–43.
- Hwang, B., Lee, J., Kim, D., Kim, J., 2021. A study on the use of grid-based spatial information for response to typhoons. *Kosdi* 17 (1), 25–38.
- Jelinek, S., Milošević, P., Rakicević, A., Petrović, B., 2021. Forecasting Sovereign Credit Ratings Using Differential Evolution and Logic Aggregation in IBA Framework (August). In International Conference on Intelligent and Fuzzy Systems. Springer, Cham, pp. 506–513 (August).
- Joo, H., Choi, C., Kim, J., Kim, D., Kim, S., Kim, H.S., 2019. A Bayesian network-based integrated for flood risk assessment (InFRA). *Sustainability* 11 (13), 3733.
- Kafle, M.R., Shakya, N.M., 2018. Multi-criteria decision making approach for flood risk and sediment management in Koshi Alluvial Fan, Nepal. *JWARP* 10 (06), 596.
- Kim, J., Kim, D., Lee, M., Han, H., Kim, H.S., 2022. Determining the risk level of heavy rain damage by Region in South Korea. *Water-SUI* 14 (2), 219.
- Kim, Y.J., Lee, C.J., 2014. Analysis on channel change of the naesung river - before the Youngju Dam impoundment (1970–2011). *J. Korean Geomorphol. Assoc.* 21 (1), 17–31.
- Kurtzman, D., Navon, S., Morin, E., 2009. Improving interpolation of daily precipitation for hydrologic modelling: spatial patterns of preferred interpolators. *Hydrolog. Process. Int. J.* 23 (23), 3281–3291.
- Lai, C., Chen, X., Wang, Z., Yu, H., Bai, X., 2020. Flood risk assessment and regionalization from past and future perspectives at basin scale. *Risk Anal.* 40 (7), 1399–1417.
- Lee, C., Kim, D., 2017. Short-term change in channel morphology of the naeseong stream before the operation of Yeongju dam. *Korea Ecol. Resilient Infrastruct.* 4 (1), 12–23.
- Lee, J., Kim, S., Kim, Y., 2019. Natural disaster risk assessment in local governments for estimating disaster management resources. *Kosham* 19 (1), 331–340.

- Lee, S., Choi, Y., Yi, J., 2020. Urban flood vulnerability assessment using the entropy weight method. *Kosham* 20 (6), 389–397.
- Lee, S.H., Kang, J.E., Bae, H.J., Yoon, D.K., 2015. Vulnerability assessment of the air pollution using entropy weights: Focused on ozone. *KARG* 21 (4), 751–763.
- Li, Z., Song, K., Peng, L., 2021. Flood risk assessment under land use and climate change in Wuhan city of the Yangtze River Basin, China. *Land* 10 (8), 878.
- Ly, S., Charles, C., Degre, A., 2011. Geostatistical interpolation of daily rainfall at catchment scale: the use of several variogram models in the Ourthe and Ambleve catchments, Belgium. *Hydrol. Earth Syst. Sci.* 15 (7), 2259–2274.
- Lyu, H.M., Sun, W.J., Shen, S.L., Arulrajah, A., 2018. Flood risk assessment in metro systems of mega-cities using a GIS-based modeling approach. *Sci. Total Environ.* 626, 1012–1025.
- Ministry of Construction and Transportation (MOCT). (2004). A study on the economic analysis in flood control projects.
- Ministry of the Interior and Safety (MOIS). (2020). Methodology Development for the Estimation and Prediction of Direct and Indirect Damages/Losses from Flood and Wind Disasters.
- Mousavi, S.M., Ataei-Ashtiani, B., Hosseini, S.M., 2022. Comparison of statistical and mcdm approaches for flood susceptibility mapping in northern iran. *J. Hydrol.* 612, 128072.
- National Disaster Management Research Institute (NDMI). (2015). Construction of Fundamental Technology for Disaster Risk Assessment and Prediction(II) - Pilot Development of Urban Flood Management.
- Park, K., Lee, M.H., 2019. The development and application of the urban flood risk assessment model for reflecting upon urban planning elements. *Water-Sui* 11 (5), 920.
- Park, S.G., Kim, H.S., Lee, K.H., & Yoon, Y.N. (2005). Conceptual Study for the Potential Risk of Flood Damage Occurrence. In Proceedings of the Korea Water Resources Association Conference (pp. 850–854). Korea Water Resources Association.
- Reese, S., Ramsay, D., 2010. RiskScape: Flood fragility methodology. Wellington, New Zealand. *Natl. Inst. Water Atmos. Res.* 42.
- Scawthorn, C., Blais, N., Seligson, H., Tate, E., Mifflin, E., Thomas, W., Jones, C., 2006. HAZUS-MH flood loss estimation methodology. I: Overview and flood Hazard characterization. *Nat Hazards Rev* 7 (2), 60–71.
- Seong, J., Byun, Y., 2016. A study on the weights of the condition evaluation of rock slope used in entropy and ahp method. *J. Korean Soc. Saf.* 31 (5), 61–66.
- Steinnocher, K., Köstl, M., & Weichselbaum, J. (2011, February). Grid-based population and land take trend indicators-new approaches introduced by the geoland2 core Information Service for Spatial Planning. In NTTS conference, Brussels.
- Van Westen, C., & Yifru, Y. (2016). Caribbean handbook on risk information management.
- Wang, W.J., Kim, S., Kim, K.T., Lee, C., Kim, H.S., 2020. Analysis of applicability of grid-based spatial analysis data for flood risk assessment. *KOSHAM* 20 (6), 399–406.
- Wang, W.J., Kim, D., Han, H., Kim, K.T., Kim, S., Kim, H.S., 2023. Flood risk assessment using an indicator based approach combined with flood risk maps and grid data. *J. Hydrol.*, 130396.
- Wannous, C., Velasquez, G., 2017. United nations office for disaster risk reduction (unisdr)—unisdr's contribution to science and technology for disaster risk reduction and the role of the international consortium on landslides (icl). In *Advancing Culture of Living with Landslides: Volume 1 ISDR-ICL Sendai Partnerships 2015–2025*. Springer International Publishing, pp. 109–115.
- Yang, X., Xie, X., Liu, D.L., Ji, F., Wang, L., 2015. Spatial interpolation of daily rainfall data for local climate impact assessment over greater Sydney region. *Adv. Meteorol.* 2015, 1–12.
- Yu, I., Kim, H., Jeong, S., 2018. Grid-based flood risk mapping considering indices of regional characteristics. *Kosham* 18 (7), 513–524.
- Zhang, D., Shi, X., Xu, H., Jing, Q., Pan, X., Liu, T., Hou, H., 2020. A GIS-based spatial multi-index model for flood risk assessment in the Yangtze River Basin, China. *Environ. Impact Assess.* 83, 106397.